A Probabilistic Analysis of the Dynamics and Predictability of Tropical Cyclogenesis

JASON A. SIPPEL AND FUQING ZHANG*

Department of Atmospheric Sciences, Texas A&M University, College Station, Texas

(Manuscript received 23 August 2007, in final form 31 March 2008)

ABSTRACT

Using methods unique for tropical cyclone studies in peer-reviewed literature, this study examines the dynamics and predictability of a nondeveloping tropical disturbance in the Gulf of Mexico during the 2004 hurricane season. Short-range ensemble forecasts are performed with a mesoscale model at low resolution with parameterized moist convection and at high resolution with explicit convection. Taking advantage of discrepancies between ensemble members, statistical correlation is used to elucidate why some ensemble members strengthen the disturbance into a tropical cyclone or hurricane and others do not.

It is found that the two most important factors in the initial conditions for genesis in this case are the presence of deep moisture and high CAPE. These factors combine to yield more active initial convection and a quick spinup during the first 6–12 h. Because these factors result in quicker genesis in some ensemble members than others, they are also the primary source for spread early in the ensemble. Discrepancies after 12 h are amplified by differences in convection that are related to fluxes of sensible and latent heat. Eventually the wind-induced surface heat exchange mechanism results in even larger ensemble spread.

1. Introduction

Understanding uncertainties associated with predicting tropical cyclone formation and subsequent intensification is important since forecasting cyclogenesis remains a challenge and intensity forecast skill significantly lags that of track forecasts (e.g., DeMaria and Gross 2003; Emanuel 2003; DeMaria et al. 2005; and others). Significant progress has recently been made in tropical cyclone track forecasts, and the current 48-h position forecast is as accurate as a 24-h forecast 10 years ago (Franklin 2005). However, there has been virtually no improvement in our ability to predict hurricane intensity (Elsberry et al. 2007), and predictions of tropical cyclone formation, rapid intensification, and decay remain particularly problematic (Houze et al. 2007).

a. Moist convection and intensity uncertainty

The primary reason for lagging forecast skill is that warm-season precipitation, whose associated dynamics play a critical role in tropical cyclone genesis and intensification (e.g., Krishnamurti et al. 2005; Hendricks et al. 2004; Montgomery et al. 2006), generally remains the least accurate forecast element at all scales (Olson et al. 1995). Islam et al. (1993) and Snyder and Zhang (2003) demonstrated that errors grow rapidly at convective scales in weakly forced warm-season events, and such error growth in the presence of moist convection can significantly impact mesoscale predictability (Zhang et al. 2002, 2003, 2006a, 2007). Focusing on an extreme warm-season precipitation event, Zhang et al. (2006a) showed that undetectable random noise contaminates deterministic warm-season mesoscale forecasts within as few as 36 h. They concluded that this error, in combination with the error associated with inadequate initial analyses and forecast models, necessitates the use of probabilistic (ensemble) forecasts for mesoscale systems.

b. The usefulness of ensembles

Ensemble forecasts have, indeed, shown great potential for forecasting tropical cyclones. For example, some

* Current affiliation: Department of Meteorology, The Pennsylvania State University, University Park, Pennsylvania.

Corresponding author address: Dr. Fuqing Zhang, Department of Meteorology, The Pennsylvania State University, University Park, PA 16802.
E-mail: fzhang@psu.edu

DOI: 10.1175/2008JAS2597.1

studies (e.g., Krishnamurti et al. 2000; Goerss 2000; Aberson 2001; Vijaya Kumar et al. 2003; Williford et al. 2003; Weber 2003, 2005a,b) have demonstrated that scalar position and intensity forecasts computed from multimodel ensembles are better than those from individual ensemble members. Additional work (e.g., Krishnamurti et al. 1997; Zhang and Krishnamurti 1999; Mackey and Krishnamurti 2001) has shown that the ensemble mean from an individual model can significantly improve on deterministic forecasts of tropical cyclones.

Ensemble forecasts have also proven useful for investigating dynamics in a wide variety of atmospheric systems, and they might be useful for investigating and diagnosing the source of forecast uncertainty in tropical cyclogenesis. Zhang (2005) used ensembles to investigate a winter coastal cyclone and found that initially random perturbations evolved into coherent structures with spatial correlation (and covariance) between forecast variables. The correlation (covariance) was highly structured and found to be greatest in the region of strong cyclogenesis and along the upper level front. In another example, Hakim and Torn (2008) expanded upon the methods of Zhang (2005) to investigate the formation dynamics of a spring continental cyclone. They used the strong covariance between variables to infer relationships between the surface cyclone and preceding upper-level disturbances and to predict changes in the cyclone strength given certain changes to the initial conditions. Finally, Hawblitzel et al. (2007, hereafter HZ07) examined mesoscale convective vortex (MCV) formation dynamics and predictability using an ensemble. They found that small initial perturbations of model forecast variables resulted in large ensemble spread such that some members produced a very strong MCV while others produced no MCV at all. The ensemble members that produced a stronger MCV had more prolific convection as early as 24 h before the MCV developed. They concluded that the intimate dependence of every aspect of MCV development on moist convection largely explained the significant forecast uncertainty associated with this event.

c. *Tropical cyclone formation: Observations and theory*

The environments in which tropical cyclones form and intensify are well documented. Riehl (1954) recognized that tropical cyclones form from preexisting disturbances over a relatively warm ocean, and Gray (1968, 1975) noted that developing disturbances are associated with large values of absolute vorticity, weak vertical wind shear, and mean upward motion. McBride and Zehr (1981) also found that tropical cyclones proceed from cloud clusters in an environment of high low-level vorticity, and Emanuel (1989) demonstrated the importance of deep moisture. In a more recent study, DeMaria et al. (2001) found that tropical cyclones are able to intensify when the 200–850-hPa zonal wind shear is less than 12.5 m s^{-1}. Other studies, such as Dunion and Velden (2004), have shown how regional phenomena (e.g., Saharan air layers in the Atlantic basin) can affect a number of the above factors and strongly modulate tropical cyclone formation and intensification. In addition to using measures of vertical wind shear, low-level vorticity, and deep moisture, the National Oceanic and Atmospheric Administration (NOAA) Satellite Services Division (SSD) also uses cloud top temperature, a proxy for sustained deep convection, and vertical instability (NOAA SSD 2008) to operationally predict tropical cyclone formation.

Emanuel (1986) and Rotunno and Emanuel (1987) pioneered a theory in which tropical cyclones intensify from an initial vortex due to positive feedback between oceanic heat fluxes and surface wind speeds. In this theory, coined wind-induced surface heat exchange (WISHE) (e.g., Emanuel et al. 1994), winds associated with a surface vortex enhance fluxes of sensible and latent heat from the ocean surface. This can lead to more vigorous convection, stronger diabatic heating, and a greater surface pressure deficit due to hydrostatic pressure falls in the vicinity of the convection. With a stronger surface pressure gradient, wind speeds and heat fluxes are higher, thus completing the loop.

While WISHE adequately describes cyclone maintenance and intensification, several requirements must be met for the process to proceed efficiently. In particular, an initial warm-core vortex of sufficient amplitude must be encompassed by ample deep-layer moisture (Rotunno and Emanuel 1987; Emanuel 1989). If sufficient moisture is not present through the midtroposphere, then convection will have the propensity to produce cold convective downdrafts and stabilize the lower troposphere.

A number of observational studies have proposed midlevel vortex merger as a means of strengthening surface vorticity and initiating WISHE. Harr et al. (1996), Simpson et al. (1997), and Ritchie and Holland (1997) observed that MCVs that form in stratiform precipitation areas of tropical mesoscale convective systems sometimes merge to produce stronger, deeper, and wider circulations than those associated with any individual vortex. This process can enhance low-level vorticity and strengthen a tropical disturbance.

Hendricks et al. (2004) and Montgomery et al. (2006) presented a different view in which surface-based convection is key to generating the tropical cyclone vortex.

In this view, system-scale deep convection drives a toroidal circulation, which itself organizes the vortex angular momentum. Individual mesoscale, low-level vortices generated by intense subsystem-scale convection (vortical hot towers, or VHTs), can also enhance the genesis process. Reasor et al. (2005) and Sippel et al. (2006) provided observational evidence of VHTs during tropical cyclogenesis, and the results of Tory et al. (2006a,b) support the idea that organized, surface-based convection may be sufficient to generate a tropical cyclone vortex.

An alternative view sharing common ideas with each of the preceding theories focuses on the thermodynamics of the incipient vortex. In this view, first proposed by Bister and Emanuel (1997) and supported by Raymond et al. (1998), convection increases midlevel relative humidity and vorticity *before* the establishment of the tropical cyclone vortex. Furthermore, the modeling study of Nolan (2007) suggests that such changes are *necessary* before any VHT process can establish a sustained, small-scale, low-level vortex. Increasing midlevel moisture allows the ratio of downdrafts to updrafts to lower significantly before genesis, and increasing midlevel vorticity allows deep convective towers to more efficiently heat the atmosphere and create a vortex. Finally, Nolan et al. (2007) similarly found in a modeling study that large-scale thermodynamics determine the rate of tropical cyclone formation.

This study uses ensemble forecasts to study the predictability and dynamics of a nondeveloping low pressure system near the Florida Keys in July 2004. The lack of predictability associated with the 2004 system provides much of the motivation for this research. The synoptic background behind this case will be established in section 2. Section 3 describes the experiment and methodology, and section 4 describes the ensemble performance and predictability in general. An analysis of the dynamics in terms of correlation structure and how the correlation relates to individual ensemble members can be found in section 5, and sensitivity experiments are investigated in section 6. A discussion of the results in the context of previous research is given in section 7. Finally, a summary and conclusions can be found in section 8.

2. Synoptic background

The disturbance that spawned the cyclogenesis of interest appeared in surface observations as a shear axis beginning on 27 July 2004 as it approached the Bahamas (not shown). The shear axis, which was the surface reflection of an upper-level potential vorticity (PV) anomaly (Fig. 1g), continued westward and crossed the Florida peninsula into the Gulf of Mexico on 28 July. The National Centers for Environmental Prediction (NCEP) global final (FNL) analysis from 0000 UTC 29 July clearly shows the surface (Fig. 1a) and 500-hPa (Fig. 1g) troughs moving over the west coast of Florida.

The synoptic background was somewhat favorable for tropical cyclogenesis from 29 to 30 July, and the National Hurricane Center mentioned the potential for development in their tropical weather outlooks. The disturbance was encompassed by ample moisture at 700 hPa (Figs. 1d,e), and a similar moisture distribution was present from the surface through 500 hPa (not shown) over the southern and southeastern Gulf. Rawinsondes from the Florida peninsula and Key West (not shown) taken on 29–30 July reveal that the environment was also unstable and favorable for deep convection. Convective available potential energy (CAPE) was generally between 1500 and 2000 J kg^{-1}, and weak synoptic ascent ($\sim$0.5 cm s^{-1}) associated with the disturbance helped reduce convective inhibition to less than 10 J kg^{-1} over the southern Florida peninsula and Florida Keys. FNL analyses during the same period show that CAPE over the Gulf of Mexico was generally between 1000 and 2000 J kg^{-1} (not shown). In response to the presence of the disturbance in a favorable thermodynamic environment, widespread convection was evident in infrared satellite imagery (not shown) as the system moved from east of Florida into the Gulf of Mexico. Finally, one neutral to slightly negative factor was that 200–850-hPa wind shear values near the circulation center were between 12.5 and 15.0 m s^{-1} (Figs. 1k–m), which is just above the favorable limit for wind shear.

Although the 2004 disturbance appeared to be in a marginally favorable environment, it never became a tropical depression. Amid prolific deep convection, the system intensified somewhat on 29 July when 700-hPa heights fell slightly (cf. Figs. 1d,e) and a closed low-level circulation developed (cf. Figs. 1a,b). Despite the closed circulation and continuing convection, the system was never sufficiently organized to attain depression classification, and by 0000 UTC 1 August it degenerated into an open wave (not shown). The failure to develop after 30 July might be related to a decrease in midlevel moisture over the center (Fig. 1f) and the nearby slightly unfavorable shear values (Figs. 1k–m).

3. Methodology

This study largely follows the methods of HZ07 by using the dynamics behind the evolution of the nondeveloping cyclone to explain the predictability of the incipient disturbance. To expand on HZ07, this investigation also uses multiple ensembles to elucidate some possible effects of cumulus parameterization and the

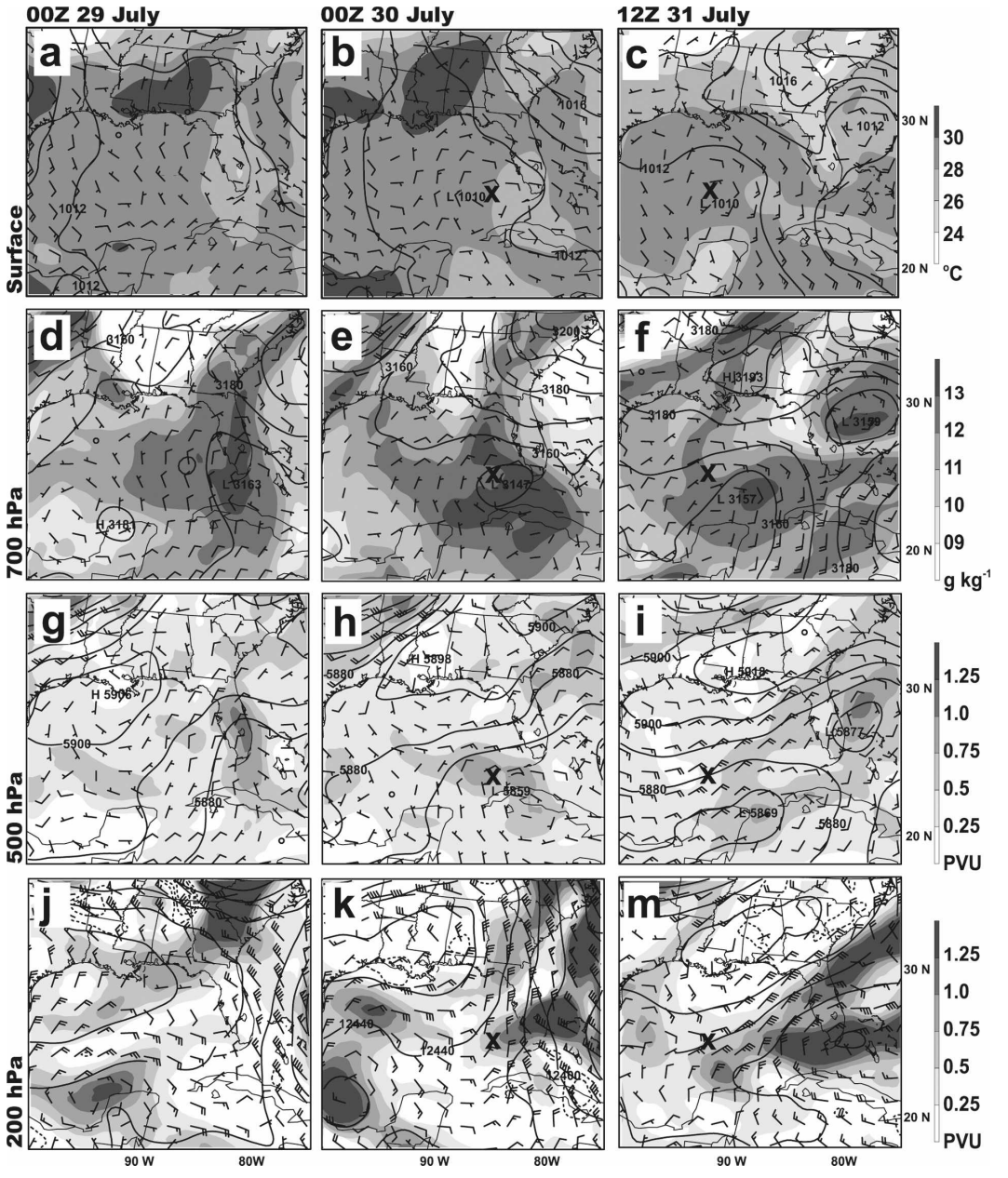

FIG. 1. FNL analyses are shown from 29 to 31 July 2004: (first row) SLP (contoured every 1 hPa), surface winds (full barb represents 5 m s^{-1}), and surface temperature (filled every 2°C); (second row) 700-hPa heights (contoured every 10 m), cloud water mixing ratio (filled every 1 g kg^{-1}), and winds; (third row) 500-hPa heights (contoured every 10 m), PV [filled every 0.25 PV units (PVU, where 1 PVU = 10^{-6} m^2 s^{-1} K kg^{-1})], and winds; (fourth row) 200-hPa heights (contoured every 20 m), PV, and 200–850-hPa wind shear. The bold **X** in the two rightmost columns represents the location of the surface circulation center.

response to subtle changes in the initial ensemble mean that result in weaker and stronger cyclones.

a. Forecast model

All experiments utilize version 3 of the fifth-generation Pennsylvania State University–National Center for Atmospheric Research (NCAR) Mesoscale Model (MM5) (Dudhia 1993) to capture the evolution of the initial disturbance. With the exception of the addition of a third nested domain, the model setup and physics in this study closely follows that of HZ07. The control experiment (CTRL) uses an outer domain with 30-km horizontal grid spacing and two nested domains with 10-km and 3.3-km grid spacing. The outer domain

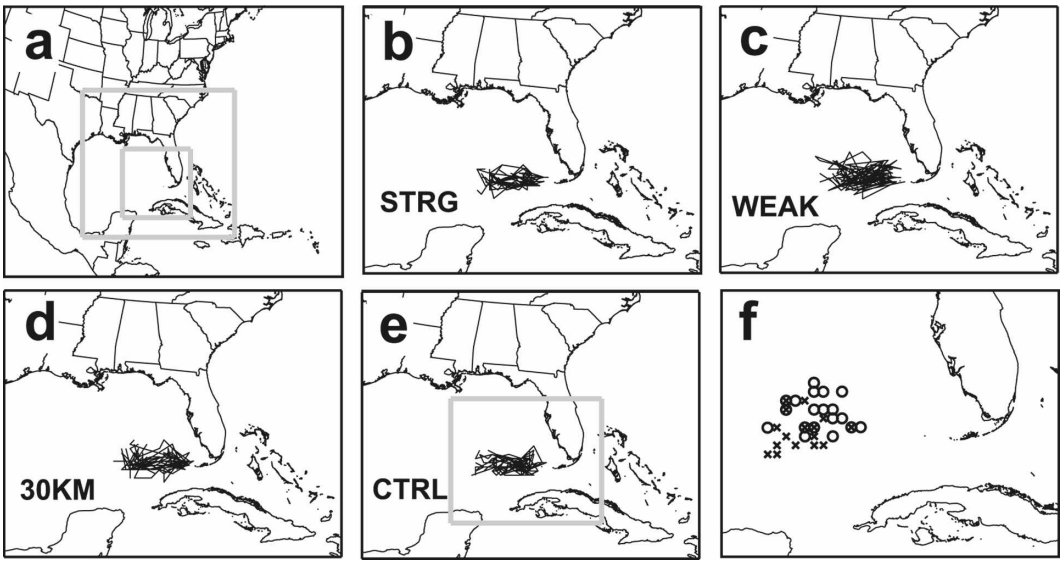

FIG. 2. (a) Model domain for all experiments and nests for the high-resolution experiment: the panel exactly encompasses the coarse grid, and the fine grids are shown in gray. The tracks of circulation centers in (b) STRG, (c) WEAK, (d) 30KM, and (e) CTRL are shown with the 10-km grid area exactly encompassed. The gray box in (e) represents the 3-km domain. (f) The 36-h positions in 30KM (bold open circle) and CTRL (bold ×) in a region exactly encompassed by the 3.3-km domain.

has 190 × 120 grid points, the middle nest uses 241 × 181 grid points, and the fine nest uses 316 × 361 grid points. The size and location of the nests (shown in Fig. 2a) are such that the 3.3-km nest adequately encompasses the genesis and subsequent tracks of the MM5-generated storms. All domains have 27 terrain-following vertical layers, and the initial and boundary conditions are supplied by the 1° × 1° FNL analysis. The Mellor–Yamada planetary boundary layer (PBL) scheme (Mellor and Yamada 1982) and Reisner microphysics scheme (Reisner et al. 1998) are used, and the model is initialized at 0000 UTC 30 July 2004 and integrated for 36 h. Although choosing a different start time does not seem to appreciably affect the ensemble spread discussed in section 4, the results of sections 5 and 6 might change with model initiation time owing to the possibility of flow-dependent dynamics. Investigating this possibility is beyond the scope of the current study. Finally, to be consistent with other experiments, all postanalysis of CTRL is performed on its coarse domain.

Sea surface temperatures are prescribed according to the FNL skin temperature, which could possibly affect results. It is well known that skin temperatures can overestimate the effective mean temperature of the ocean mixed layer, which might explain why many ensemble members forecast more strengthening than observed. Also, tropical cyclones have been observed to decrease sea surface temperatures from 1° to about 6°C (Black 1983; Bender et al. 1993) in their wakes. While the wake effect should generally be negligible for very weak storms, it is possible that it would change results for a few of the ensemble members with stronger cyclones discussed in section 4.

Sensitivity experiment 30KM utilizes only the outer 30-km domain to investigate whether qualitatively similar results to CTRL can be obtained with cumulus parameterization. Integration again starts at 0000 UTC 30 July 2004, and the model physics are the same as in CTRL with the exception that the Grell cumulus scheme (Grell et al. 1991; Grell 1993) is used. As with the other physics options, the Grell scheme was chosen to be consistent with HZ07. Although this choice is somewhat arbitrary, this scheme is occasionally used in simulations of tropical cyclones (e.g., Park and Zou 2004; Braun et al. 2006; Braun 2006; Wu et al. 2006).

b. Ensemble initialization

This study uses ensembles of 20 members, which is a sufficient number according to the results of Zhang (2005). The ensemble initial conditions of CTRL/30KM were created by perturbing the FNL analysis with random, balanced noise derived from the NCEP background error statistics implanted in the MM5 three-dimensional variational data assimilation system (Barker et al. 2004). Figure 3 shows the vertical distribution of the initial ensemble spread in CTRL/30KM, which is 0.7–1.2 m s^{-1} for zonal wind, 0.3–0.6 K for temperature, and 2%–4% for relative humidity.

The initial spread of CTRL/30KM in Fig. 3 appears

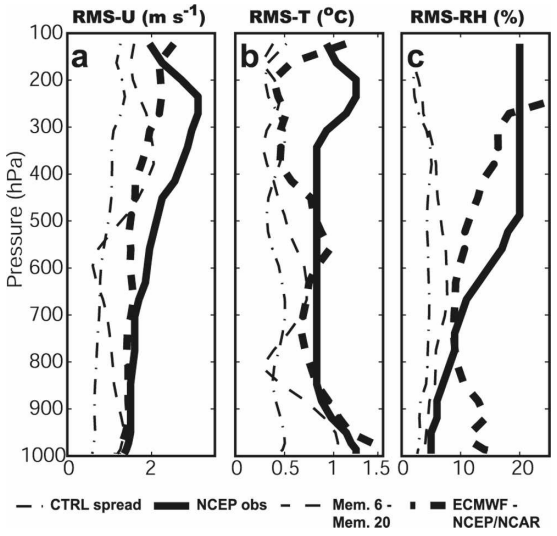

FIG. 3. The initial rms spread of (a) zonal wind, (b) temperature, and (c) relative humidity for CTRL (thin dashed–dotted lines). Also shown are the NCEP-assumed error for rawinsondes (thick solid lines), the rms difference between the ECMWF operational analysis and the NCEP–NCAR reanalysis (thick dashed lines), and the rms difference between members 6 and 20 of CTRL (thin dashed lines).

conservative when compared to other measures of error largely because the ensemble initialization method used here introduces only large-scale uncertainties, and other quantities in Fig. 3 include all error scales. For example, the spread is smaller than both NCEP-assumed sounding observational error and the root-mean-square (rms) difference between the NCEP–NCAR 2.5° × 2.5° reanalysis and the European Centre for Medium-Range Weather Forecasts 2.5° × 2.5° operational analysis over the MM5 domain at the initial time. The rms difference between the FNL analysis and both the ECMWF analysis and the NCEP–NCAR reanalysis (not shown) is also significantly larger than the spread of CTRL/30KM. Since the rms difference between various analyses can be used as a rough estimate of typical analysis error at lead operational centers, the spread is also smaller than the typical analysis error. In addition to the lack of smaller scale error, model error is not considered, and boundary conditions are not perturbed here. These additional sources of error may lead to even stronger forecast divergence and thus further limit hurricane predictability.

In addition to 30KM, sensitivity experiments WEAK and STRG were created to determine the effect of changing the initial conditions to produce stronger and weaker cyclones. These experiments use the same 30-km domain and model physics as 30KM. In WEAK and STRG, ensembles of initial conditions were generated by respectively perturbing (in the same manner as

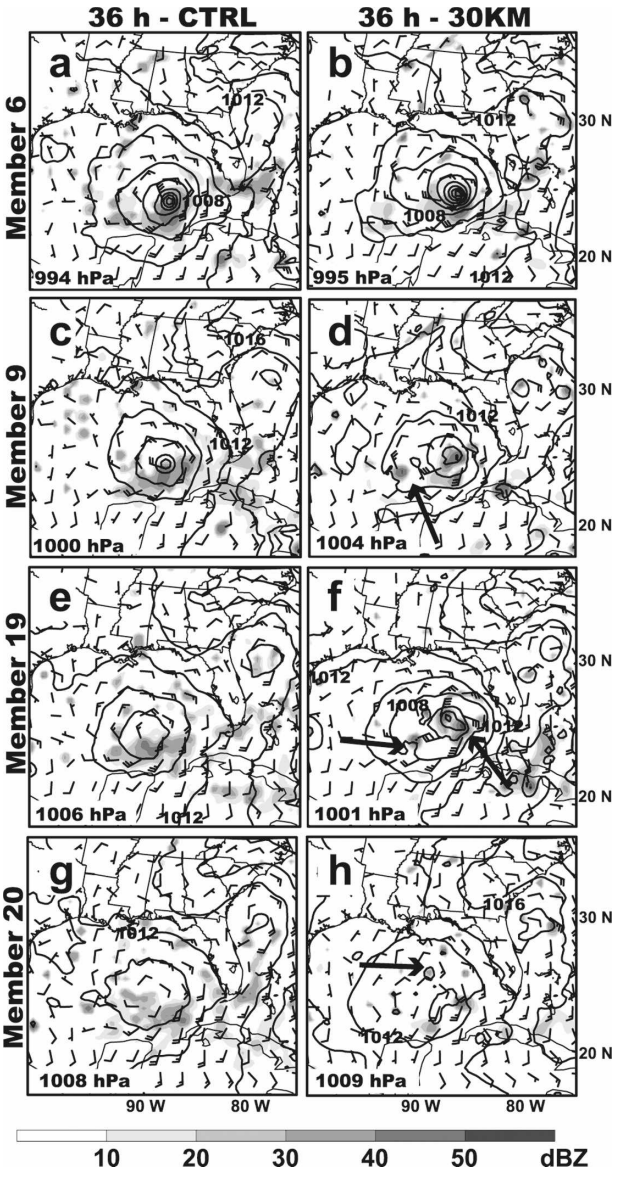

FIG. 4. Simulated radar reflectivity (shaded every 10 dBZ), sea level pressure (contoured every 10 hPa), and surface winds (full barb represents 5 m s^{-1}) for select members of CTRL and 30KM at 36 h. Arrows point to intense convective towers (mentioned in text) that significantly alter the local environment. The minimum SLP for each member is shown in the bottom left corner of each panel.

CTRL/30KM) the initial conditions of members 20 and 6 from ensemble CTRL/30KM. Members 6 and 20 are on opposite ends of CTRL/30KM in terms of cyclone strength, and their relative strengths can be judged by the forecasts of surface pressure, wind, and reflectivity shown in Fig. 4. The cyclone in member 6 (Figs. 4a,b) is generally one of the strongest in the ensemble while the storm in member 20 (Figs. 4g,h) is generally the weakest.

TABLE 1. Confidence intervals (CI) for varying degrees of statistical confidence for the correlation r values indicated.

CI	$r = 0.1$	$r = 0.3$	$r = 0.5$	$r = 0.7$	$r = 0.85$
99%	(−0.48, 0.62)	(−0.30, 0.73)	(−0.07, 0.83)	(0.24, 0.90)	(0.56, 0.95)
95%	(−0.36, 0.52)	(−0.16, 0.66)	(0.07, 0.77)	(0.37, 0.87)	(0.65, 0.94)
90%	(−0.29, 0.46)	(−0.09, 0.61)	(0.15, 0.74)	(0.44, 0.85)	(0.69, 0.93)
80%	(−0.21, 0.39)	(0.00, 0.55)	(0.23, 0.70)	(0.51, 0.74)	(0.74, 0.92)

c. Uncertainty and/or predictability

The root mean of difference total energy (RM-DTE) is used here to investigate forecast uncertainty. The form of DTE used here is a commonly used measure of the predictability in ensembles (e.g., Mitchell et al. 2002; Zhang et al. 2006b; Meng and Zhang 2007; HZ07), and it is calculated as

$$\mathrm{DTE} = 0.5(u'u' + v'v' + kT'T'). \quad (1)$$

In this equation the prime denotes the difference between a member and the ensemble mean, u and v are the zonal and meridional velocity components, T is the temperature, and $k = C_p/T_r$ ($C_p = 1004.9$ J kg^{-1} K^{-1} and $T_r = 270$ K). RM-DTE is calculated via

$$\mathrm{RM-DTE}_{i,j} = \sqrt{\frac{1}{N_e}\sum_{N=1}^{N_e}\frac{1}{k_{\max}}\sum_{k=1}^{k_{\max}}\mathrm{DTE}_{i,j,k,N}}, \quad (2)$$

where i and j are horizontal gridpoint indices, $k_{\max}$ is maximum vertical extent of the model domain, and N is the ensemble member index. Although this form of DTE does not account for differences in mixing ratio or vertical velocity, the spatial distribution of ensemble spread in these variables is qualitatively similar to that in u, v, and T. Therefore, alternate forms of DTE that account for differences in these variables are qualitatively similar to that shown here.

d. Correlation analysis

As in HZ07, the correlation between different forecast variables is investigated to understand the predictability and to study relationships between variables within the ensembles. The linear correlation coefficient r is calculated among a set of N data points using

$$r(x_{ijk},y_{ijk}) = \frac{\dfrac{1}{N-1}\displaystyle\sum_{n=1}^{N}(x_{ijk,n} - \overline{x_{ijk}})(y_{ijk,n} - \overline{y_{ijk}})}{\left[\dfrac{1}{N-1}\displaystyle\sum_{n=1}^{N}(x_{ijk,n} - \overline{x_{ijk}})^2\right]^{1/2}\left[\dfrac{1}{N-1}\displaystyle\sum_{n=1}^{N}(y_{ijk,n} - \overline{y_{ijk}})^2\right]^{1/2}}, \quad (3)$$

where x and y denote two model-state variables and i, j, and k represent three-dimensional grid points. Verbal descriptions of the correlation will follow those of HZ07 with the exception that correlation above 0.85 is described as very strong. Correlation between 0.7 and 0.85 is described as strong, between 0.5 and 0.7 as moderate, and between 0.3 and 0.5 as weak. Values below 0.3 are described as uncorrelated. In the framework of statistical significance with a sample size of 20, a correlation of 0.7 is statistically different from 0 with over 99% confidence, whereas 0.5 and 0.3 are respectively different from 0 with roughly 95% and 80% confidence.

This study also compares statistics of different ensembles, so it is useful to understand which differences in correlation are statistically significant and which are not. Because correlation confidence interval (CI) lengths vary with correlation and the intervals themselves are not symmetric for smaller sample sizes, Table 1 has been included to give CIs for relevant correlation values with a sample size of 20. Generally speaking, differences between strong and weak correlation are associated with fairly high confidence, as are differences between moderate and very strong correlation. However, differences between moderate and strong correlation have lower confidence, and differences between weak and moderate correlation are insignificant. This being the case, care must be taken not to draw conclusions based on small differences, especially for weaker correlation.

Because many of the variables investigated in this study are correlated with multiple other variables, statistical control is sometimes used to elucidate the correlation between two variables while effectively holding a third variable constant. For example, if variables A, B, and C are all correlated, then (A: B) is the correlation between A and B, and (A: $B|C$) is the cor-

relation between A and B when controlling for C. The controlled correlation is calculated by removing the variation in B that results from its relationship with C. In other words, linear regression between B and C is first used to predict values of B given C, and the residuals between the actual and predicted values of B are then calculated. Finally, A is correlated to the residuals to compute the controlled correlation (A: $B|C$).

This study mostly examines correlation of variables averaged over spatial areas in order to gain insight into dynamics. For example, in many cases correlation is between SLP at 36 h (when the ensemble-mean strength is greatest) and variables at earlier times. In any case, SLP and other metrics of storm intensity (i.e., surface vorticity and wind speed) are averaged over an 11×11 grid point, 300×300 km^2 area surrounding the center. Unless otherwise specified, other variables are horizontally averaged over a 21×21 grid point, 600×600 km^2 area also centered on the storm center.

Because the developing cyclones take very different tracks (e.g., Fig. 2), correlation analysis is completed in a Lagrangrian framework wherein the subjectively determined meso-α circulation center within every ensemble member is centered on the same point. At some times in various ensemble members, a closed circulation center does not exist. In that circumstance, the center of the problematic member(s) is (are) defined by the low-level vorticity maximum that is also consistent with the track of the cyclone at previous and later times. Note that the following correlation analysis is not particularly sensitive to the *exact* definition of the center, so subjective errors have no impact on the results.

Since surface pressure falls are related to net latent heat release (and thus net precipitation) in each conceptual model for tropical cyclone development, much of the correlation analysis here also focuses on the correlation between precipitation totals and various fields (e.g., SLP) that are affected by or affect precipitation and/or latent heating. To compute precipitation totals in the Lagrangian framework, forecast precipitation in the Eulerian framework is first divided into totals over 6-h increments. To move from the Eulerian framework to a Lagrangian framework, 6-h precipitation totals are averaged over a 21×21 grid point box surrounding the location of the center at the end of each 6-h period. The averaging area is large enough that the precipitation shields associated with the developing cyclones are mostly contained within their respective averaging areas for each 6-h period.

Finally, the reader should be aware of semantics and convention that affect interpretation. For example, because tropical cyclone intensity is generally negatively correlated with SLP, the correlation analyses here use the negative of SLP instead of SLP so that the correlation will be in a positive sense to the intensity of the storm. Furthermore, "intensity" and "SLP" are used interchangeably.

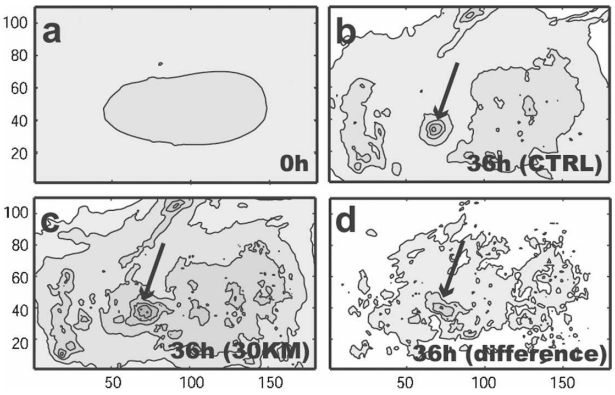

FIG. 5. RM-DTE of CTRL and 30KM calculated according to Eq. (2), contoured every 1 m s^{-1}: Axis scales are in model grid points. (a) The analysis (0-h) RM-DTE for both ensembles; (b), (c) 36-h RM-DTE and (d) 36-h difference in RM-DTE between the two ensembles. The arrows point to the genesis region.

4. Ensemble performance and predictability

Ensemble spread in CTRL grows rapidly as a result of ensemble members strengthening the incipient cyclone at different rates and moving it in different directions. The left column of Fig. 4 shows that by 36 h, there is a wide variety of forecasts within the ensemble. Recall that member 20 forecasts minimal pressure falls until this time (Fig. 4g), and member 6 has a strong tropical storm (Fig. 4a). The evolution of RM-DTE in CTRL (Fig. 5) shows that ensemble spread grows substantially in the vicinity of the cyclone forecast track (the arrows in Fig. 5 point to the genesis region). For example, the absolute maximum horizontal RM-DTE increases from about 2 m s^{-1} at the analysis time (Fig. 5a) to over 5 m s^{-1} at 36 h (Fig. 5b). Vertical profiles of RM-DTE (not shown) indicate that error growth is similar throughout the entire lower troposphere and somewhat stronger above 200 hPa.

RM-DTE at 36 h is significantly less in CTRL than in 30KM in the vicinity of the cyclone (Fig. 5), a likely result of how Grell cumulus parameterization treats convection. Low-resolution runs with Grell produce more intense convective cells and less stratiform precipitation than simulations with only explicit convection. For example, Fig. 6 shows that far more grid points in CTRL attain weaker values of reflectivity (i.e., 25–35 dBZ), as expected in stratiform precipitation, whereas more points in 30KM attain higher values of reflectivity, as expected in convective cells. One result is that

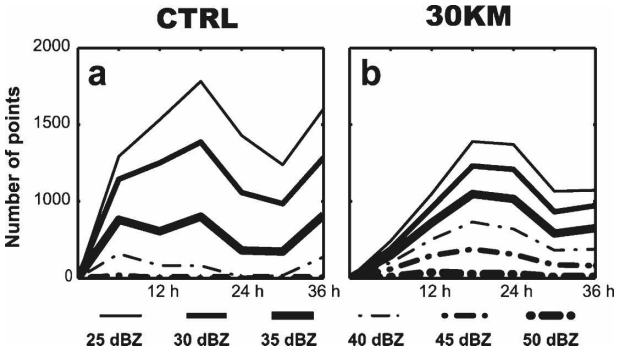

FIG. 6. The number of grid points summed over all ensemble members that attain threshold values of maximum reflectivity near the cyclone center in CTRL and 30KM. The analysis is completed in a 21 × 21 gridpoint box centered on the cyclone in each member. Maximum reflectivity is calculated by finding the maximum reflectivity value in a vertical column above a given point.

the variance of precipitation totals in the vicinity of the cyclone is much higher in 30KM than CTRL (e.g., Fig. 7d). Coincidentally, the wind field around deep convective towers in the low-resolution runs is altered over a larger area than that in the high-resolution run (the arrows in Fig. 4 point to a few such examples). This is qualitatively similar to findings in Davis and Bosart (2002) and Mapes et al. (2004) that the Grell scheme is often reluctant to activate but, after activation, it tends to produce very intense rainfall and excessive perturbations to model variables.

There are slight differences in ensemble-mean cyclone intensity between CTRL and 30KM and much larger differences between WEAK and STRG. The ensemble-mean minimum 36-h SLP is 1005.2 hPa in CTRL and 1003.9 hPa in 30KM. Meanwhile, in WEAK and STRG the ensemble mean SLP is respectively 1008.2 and 998.3 hPa. The discrepancy between WEAK and STRG can also be seen in the relative accuracy of their forecasts. Roughly 25% of the members in WEAK produce quite good forecasts of no cyclogenesis out to 36 h. For example, the 36-h SLP, reflectivity, and surface wind forecast of member 14 in WEAK (Fig. 8a) shows only a weak, disorganized low in the Gulf of Mexico. The only apparent surface difference between this member and the analysis for the same time (Fig. 1c) is that the 1012-hPa isobar is closed in member 14. The impact of the closed isobar on the wind field in member 14 must be minimal because both surface circulations are similar. Meanwhile, no members of STRG produce 36-h forecasts with as weak of a surface low as member 20 in CTRL/30KM (i.e., Figs. 4g,h) or the several members in WEAK (not shown) that resemble member 14. In fact, four members in STRG have storms of hurricane intensity by 36 h (e.g., Fig. 8b).

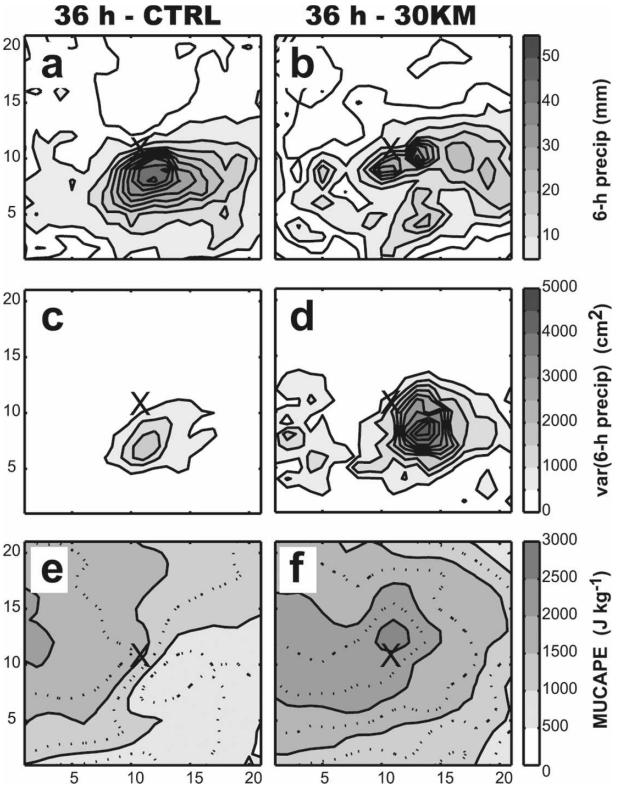

FIG. 7. (a), (b) Ensemble-mean 6-h precipitation ending at 36 h, (c), (d) variance of precipitation, and (e), (f) ensemble-mean MUCAPE at 36 h for (a), (c), (e) CTRL and (b), (d), (f) 30KM. The analysis is completed in a Lagrangian framework, and the × marks the location of the Lagrangian cyclone center. The additional line outside the shaded regions in (a) and (b) encircles areas where mean precipitation is greater than 2 mm; the dotted lines in (e) and (f) indicate intermediate values of MUCAPE in multiples of 250 J kg^{-1}.

5. Correlation analysis: The basic dynamics in CTRL

Cyclone intensity at 36 h is largely dependent upon the net latent heating and intensity of cyclogenesis during the first 12–24 h. For example, Fig. 9b shows the

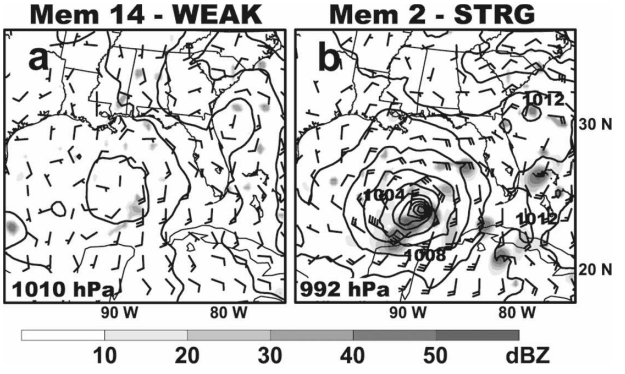

FIG. 8. As in Fig. 4, but for (a) member 14 of WEAK and (b) member 2 of STRG shown at 36 h.

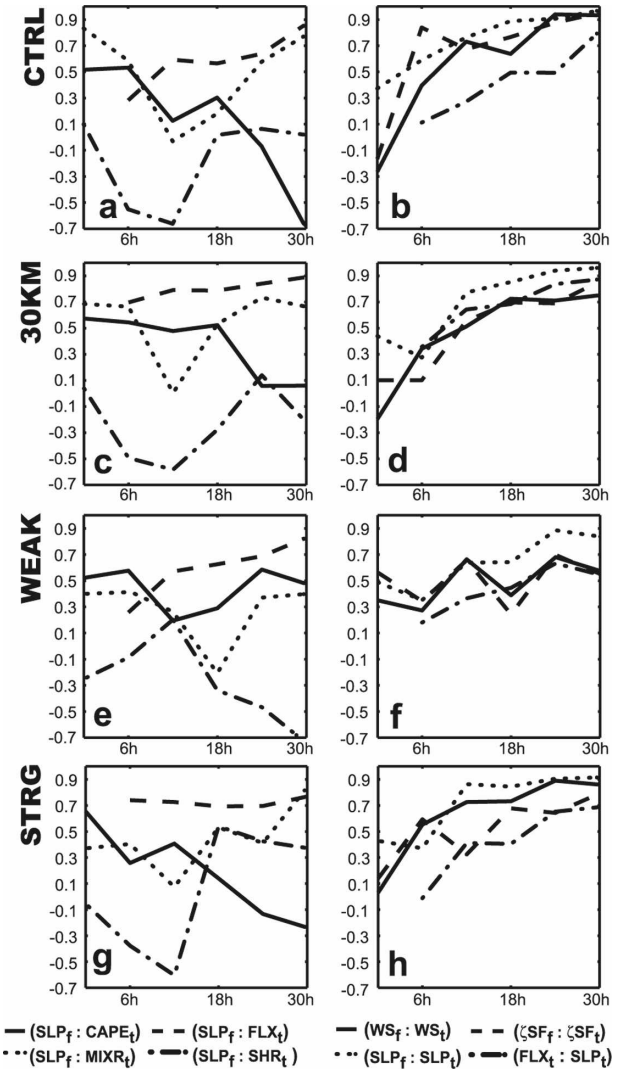

FIG. 9. Time evolution of correlation between different variables in (a)–(b) CTRL, (c)–(d) 30KM, (e)–(f) WEAK and (g)–(h) STRG. In the legends CAPE refers to MUCAPE, FLX refers to latent heat fluxes, SHR refers to 200–850-hPa wind shear, MIXR refers to 500–850-hPa mean mixing ratio, WS refers to wind speed, ζSF refers to surface vorticity: the *f* subscript represents the final forecast time, and the *t* subscript represents time. CAPE, FLX, and SHR are averaged over a 21 × 21 gridpoint Lagrangian area, and MIXR, SLP, WS, and ζSF are averaged over an 11 × 11 gridpoint Lagrangian area.

time evolution of correlation between instantaneous and final SLP, instantaneous and final surface wind speeds, and instantaneous and final surface vorticity in CTRL. By 12 h, all three variables show strong correlation with their values at 36 h, and by 24 h the correlation is very strong. Similarly, the correlation between final SLP and 12-h precipitation totals (not shown) is strong, and it becomes very strong for 24-h precipitation totals. Because differences during the first 24 h crucially determine later differences, the remainder of this study focuses especially on the first 24 h of cyclogenesis.

a. Role of deep moisture

The amount of initial moisture present throughout nearly the entire troposphere is very important for cyclogenesis in CTRL. Figure 10a, which shows the correlation between final SLP and initial variables in CTRL as a function of height, indicates significant correlation between SLP and mixing ratio from the surface to about 300 hPa. Furthermore, the mixing ratio around 700 hPa is correlated to final intensity more strongly than any other variable in the initial conditions.

Figures 11 and 12 show how the moisture correlation analysis relates to the individual members of CTRL. The bottom row of Fig. 11 shows the water vapor mixing ratio (solid contoured every 1 g kg^{-1}) at 700 hPa for the four ensemble members shown in Fig. 4. Figure 12h shows the evolution of an 11 × 11 gridpoint average of mean 500–850-hPa mixing ratio (hereafter used interchangeably with "layer-mean moisture"), and Fig. 12f shows the time evolution of area-average wind speeds near the centers of the same four members. Member 6 is the only member whose initial 700-hPa mixing ratio exceeds 10 g kg^{-1} (Fig. 11e), and it quite clearly has the most layer-mean moisture. It is also always the strongest member in terms of surface wind speeds. Members 9 and 19 have intermediate values of initial midlevel moisture, and they also have intermediate wind speeds throughout the forecast. Finally, member 20 is the only member in which the 8 g kg^{-1} isopleth encroaches upon the western edge of the genesis region (Fig. 12h), and it clearly has the lowest layer-mean moisture. It is also the only member that does not strengthen.

Although ensemble members with higher initial midlevel moisture more quickly strengthen the cyclone, it does not appear that higher initial deep moisture directly reduces the strength and/or number of downdrafts. For example, the ensemble-mean 500–850-hPa mixing ratio and surface equivalent potential temperature θ_e in Figs. 13a,b both fall substantially during the first 12 h in CTRL, and Fig. 12 shows that ensemble members with *more* initial convection drive this change. First, although surface θ_e is initially much higher in the convectively active ensemble members shown in the figure, it falls sharply in members with more convection (e.g., Figs. 12a–c). By 12 h, θ_e has equilibrated in all members shown. Furthermore, member 6 has the highest initial layer-mean moisture, but it has the lowest minimum surface θ_e near the center by 12 h (Fig. 12d). Layer-mean moisture also sharply decreases in members 6, 9, and 19 (Fig. 12h), and it thus becomes completely uncorrelated with final SLP by 12 h (Fig. 9a).

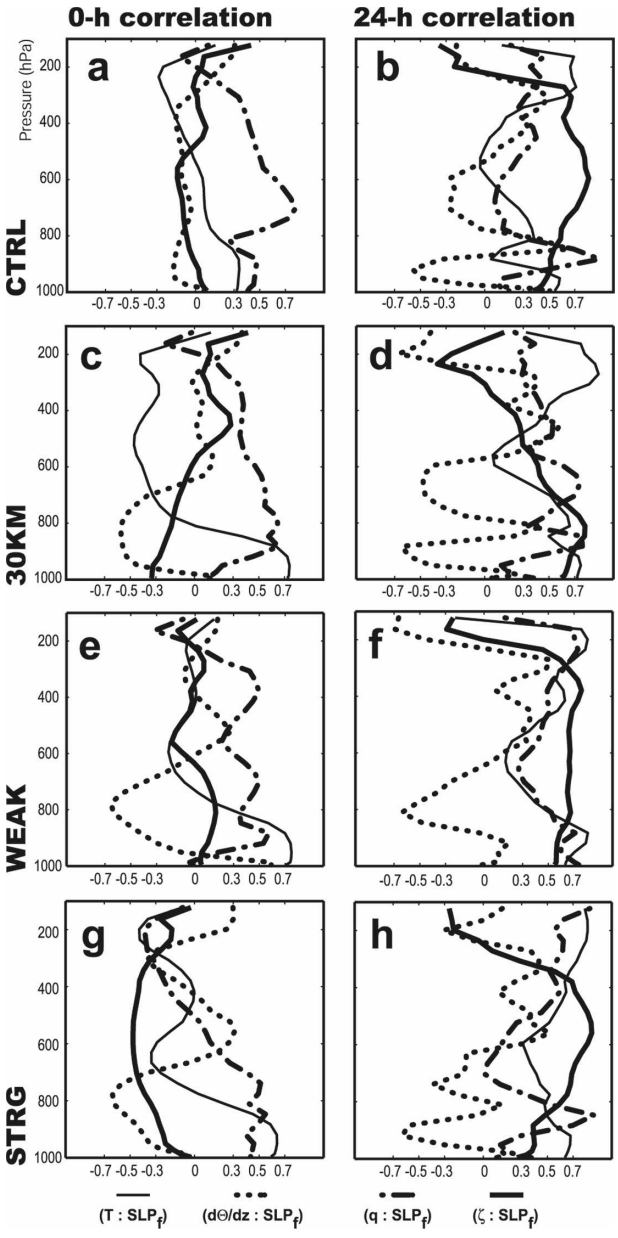

FIG. 10. Vertical profiles of correlation between final storm intensity (SLP_f) and area-averaged temperature T, mixing ratio q, static stability $\partial\theta/\partial z$, and vorticity ζ at the time indicated at the top of the columns. Variables are averaged over a 21 × 21 gridpoint Lagrangian area, and SLP is averaged over an 11 × 11 gridpoint Lagrangian area. Results are shown for (a)–(b) CTRL, (c)–(d) 30KM, (e)–(f) WEAK, and (g)–(h) STRG.

Finally, the weak correlation between initial layer-mean moisture and surface θ_e (not shown) during the first 24 h is not statistically different from that at the analysis time. Thus, any relationship between the two variables can be explained by their initial relationship, and higher initial layer-mean moisture does not dynamically alter subsequent θ_e.

It is possible that higher deep moisture directly contributes higher rates of precipitation and latent heating without reducing the number of downdrafts. In fact, some members (e.g., member 6) have so much convection that they actually appear to have stronger or more numerous mean downdrafts than ensemble members with less initial moisture and convection. This appears to be consistent with the result from Nolan (2007) that the frequency and strength of updrafts increases as midlevel moisture increases, but the frequency and strength of downdrafts does not decrease.

b. Role of convective instability

Convective instability is also an important factor for cyclone intensity, likely because of its relationship with subsequent precipitation. Area-averaged most unstable CAPE (MUCAPE)[1] is about 1750 J kg^{-1} in CTRL at the analysis time (Fig. 13c) and it is moderately correlated with final storm intensity, 0–12-h precipitation, and 0–24-h precipitation (not shown). Furthermore, the correlation between MUCAPE and final intensity does not appear to be a simple result of positive correlation between MUCAPE and another variable that favors intensification. In Fig. 14, which shows the correlation between MUCAPE and final SLP when controlling for initial variables, only initial temperature and mixing ratio below 900 hPa significantly affect the correlation. This is not surprising as PBL temperature and mixing ratio determine over 90% of the variance in MUCAPE. Also, although controlling for PBL mixing ratio and/or temperature reduces the correlation between MUCAPE and final SLP, MUCAPE is still a better predictor of final storm intensity than either of these variables individually.

Although it is not readily apparent in Fig. 11, MUCAPE in this case relates to the large-scale environment through its association with quasigeostrophic (QG) lift. The MM5 develops the cyclone in an environment of weak QG lift[2] (shaded in the bottom row of

[1] MUCAPE is computed as the CAPE for the parcel in each column with maximum equivalent potential temperature within the lowest 3000 m. Following the recommendation of Doswell and Rasmussen (1994), virtual potential temperature is used in this calculation.

[2] QG omega is calculated via 3D inversion of the Q-vector form of the QG omega equation using the domain-average Coriolis parameter and vertical stability profile. Q-vector forcing, topographic boundary condition forcing, and Ekman forcing are all considered in the inversion. For more details, see the source code of the RIP4 postprocessing program (see http://www.mmm.ucar.edu/wrf/users/docs/ripug.htm).

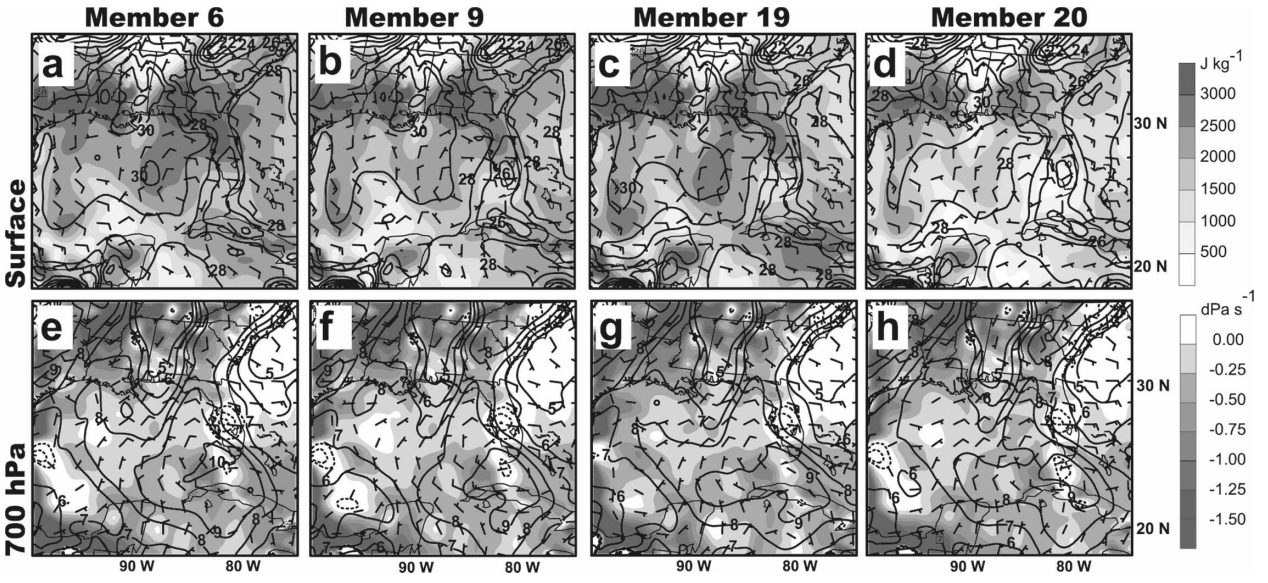

FIG. 11. Initial fields of ensemble members in Fig. 4: (top row) temperature (contoured every 2°C) and MUCAPE (shaded every 500 J kg^{-1}) along with surface wind barbs (full barb represents 5 m s^{-1}); (bottom row) 700-hPa mixing ratio (solid contour every 1 g kg^{-1}), QG vertical motion (shaded every 0.25 dPa s^{-1} for QG lift; dashed contour every 0.25 dPa s^{-1} for QG subsidence), and 700-hPa winds.

Fig. 11), which is known to reduce static stability and moisten the atmosphere. MUCAPE over the genesis region is well correlated with the strength of the QG circulation of the initial PV anomaly (not shown), and there is moderate correlation between area-averaged MUCAPE and low-level QG lift in the genesis region of CTRL. However, low-level QG lift and final SLP are not significantly correlated, so QG lift is not directly a significant contributor to storm intensity.

MUCAPE in CTRL quickly becomes uncorrelated with final SLP since convection in the ensemble significantly reduces its magnitude (e.g., Fig. 13c) and variance. The correlation between area-average MUCAPE and final SLP significantly decreases after 6 h in Fig. 9a, and area-average MUCAPE equilibrates for all ensemble members shown in Fig. 12e by about 12 h. By 30 h the members of CTRL that have high MUCAPE are those that have little convection, and the correlation between 30-h MUCAPE and precipitation over the preceding 6 h in CTRL is strongly negative (not shown). Thus, MUCAPE and final SLP become significantly anticorrelated in Fig. 9a.

Figures 11 and 12 show how the above correlation analysis relates to individual ensemble members in CTRL. The top row in Fig. 11 displays MUCAPE, again shaded every 500 J kg^{-1}, and surface temperature contoured every 2°C. In member 6 (Fig. 11a) the maximum MUCAPE slightly to the west of the genesis region is higher than in the other members. This member also has the least pronounced minimum in MUCAPE in the immediate genesis region. Meanwhile, member 20 (Fig. 11d) starts off with significantly lower initial MUCAPE and surface temperatures than the other members shown in Fig. 11. Figure 12 shows that the convective response during the first 12 h of integration is, in general, proportion to the initial area-averaged convective instability. Likewise, there is a dramatic increase in area-averaged surface wind speeds near the centers of the stronger ensemble members during the first 6 h. Thereafter, stronger ensemble members stay stronger, and weaker members stay weaker.

c. Role of vorticity and vertical wind shear

Ensemble-mean deep-layer (200–850 hPa) wind shear peaks around 6 h in CTRL (Fig. 13d), and shear from 6 to 12 h is moderately anticorrelated with final SLP (Fig. 9a). Note that the shear in Figs. 12 and 13 is again an area average, and ensemble mean shear during the first 12 h is generally in agreement with Fig. 1k. The substantially weaker shear at later times in Figs. 12 and 13 seems to have little effect on final intensity (Fig. 9a).

The dramatic decrease in shear at later times in Figs. 12g and 13d appears to be caused by convection that occurs during the first 12 h. For example, 12-h precipitation totals are strongly anticorrelated with deep-layer shear at 12 h in CTRL. Even the convection in member 20, which is weaker than that of any other ensemble member (Figs. 12a,b), is sufficient to rearrange the upper-level PV field (not shown) and

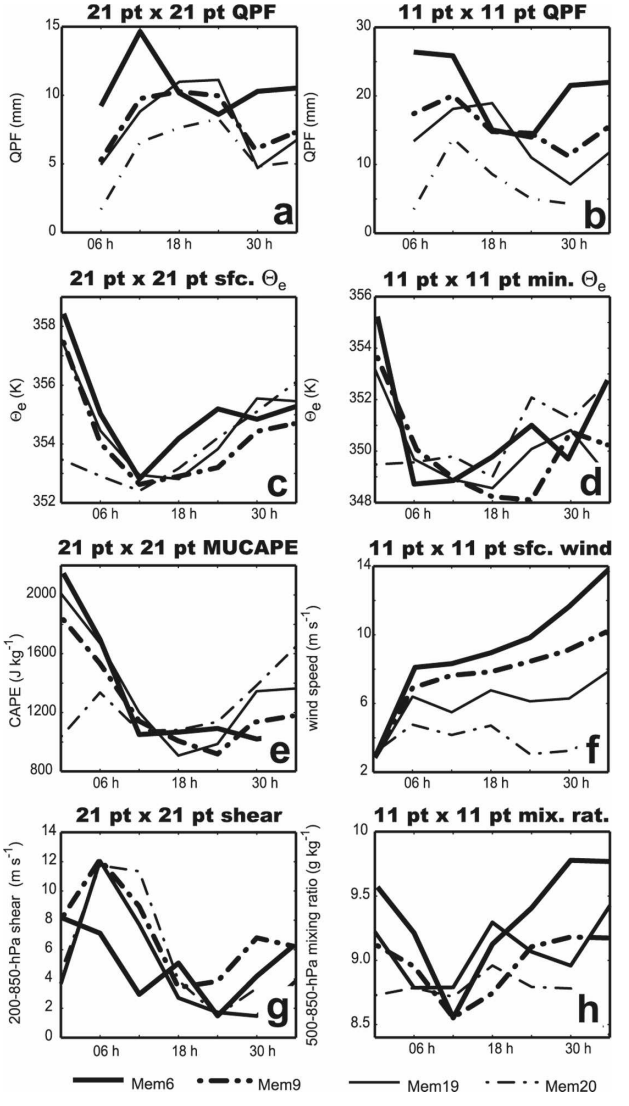

FIG. 12. Time evolution of certain quantities from the four ensemble members shown in Figs. 4 and 11: (a)–(c) Evolution of Lagrangian area-average quantities as indicated in the panel titles and (d) evolution of the minimum surface θ_e in an 11 × 11 gridpoint Lagrangian area.

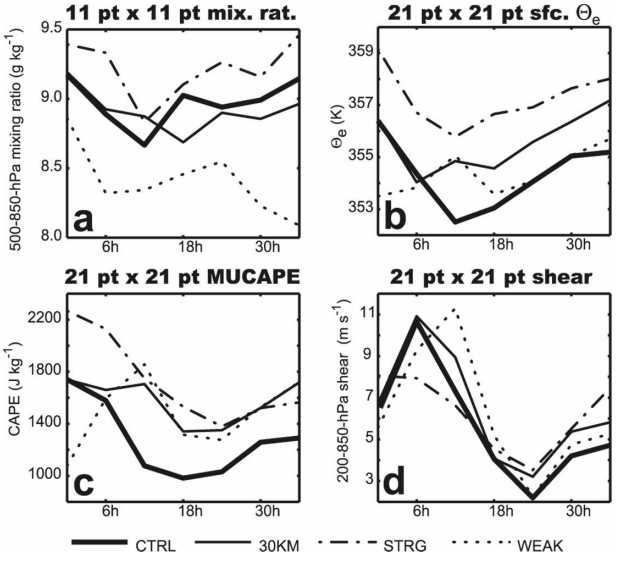

FIG. 13. The time evolution of certain quantities from Fig. 12 for the ensemble means of CTRL, 30KM, STRG, and WEAK.

reduce deep-layer shear in the genesis region by 18 h (Fig. 12g). This is incongruent with Figs. 1k–m and shows how quickly well-placed convection can lead to error in an ensemble mean. Ironically, the lower shear results in a more favorable environment for intensification.

Low-level vorticity is initially uncorrelated to final SLP in CTRL, but it quickly becomes an excellent predictor of itself. The initially insignificant correlation in Fig. 10a may indicate that the initial disturbance provides sufficient vorticity for cyclogenesis to proceed in all members. Meanwhile, 6-h surface vorticity is very strongly correlated with final vorticity in CTRL. Thus, ensemble members that are able to rapidly build a surface vortex during the first 6 h are the same members that have stronger vorticity at 36 h.

d. Initial latent heat fluxes and the onset of WISHE

It is clear from Fig. 9 that surface latent heat flux[3] (LHF) is important before WISHE becomes a dominant intensification factor in CTRL. The time-lag correlation between final SLP and area-averaged LHF (Fig. 9a) rises to moderate strength by 12 h, and area-averaged LHF over the first 12 h is weakly to moderately correlated to subsequent precipitation. Nonetheless, the instantaneous correlation between area-average LHF and SLP (Fig. 9b) is quite weak during the first 24 h. The statistical significance of LHF before 24 h is therefore not strongly tied to WISHE (see Emanuel 1986, 1989, 1995; Rotunno and Emanuel 1987), which should cause high instantaneous correlation between LHF and SLP.

WISHE appears to become an intensification mechanism by 30 h in CTRL. In Fig. 15, ensemble mean LHF is shaded, and the instantaneous correlation between LHF and storm intensity is contoured. The expanding

[3] Although WISHE theory relates to *total* heat flux (i.e, the sum of latent and sensible heat flux), latent heat fluxes in these simulations are more than an order of magnitude greater than sensible fluxes. Therefore, the correlation between storm intensity and total fluxes is determined almost exclusively by latent heat fluxes.

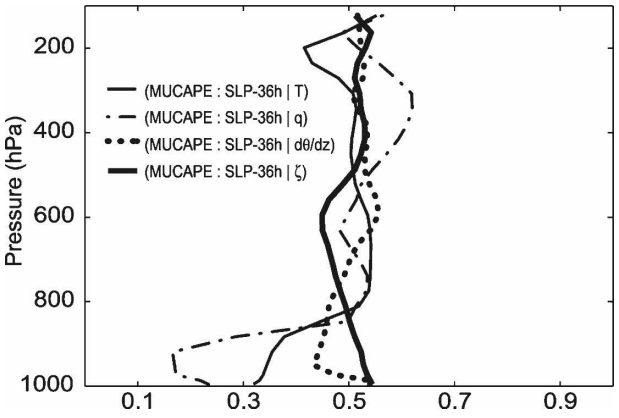

FIG. 14. Correlation between MUCAPE and final intensity (SLP-36h) when controlling for temperature T, mixing ratio q, static stability $\partial\theta/\partial z$, and vorticity ζ at different heights at the analysis time. All variables except SLP-36h are averaged over a 21×21 gridpoint Lagrangian area; SLP-36h is averaged over an 11×11 gridpoint Lagrangian area.

area of dark shading and increasingly bold contours near the center from 12 to 36 h shows that the importance of LHF increases considerably as LHF itself increases. Likewise, Fig. 9a shows that the instantaneous correlation between area-averaged LHF and SLP increases to a strong level by 30 h, consistent with WISHE becoming an intensification factor.

Concomitant with the growing importance of WISHE in CTRL, the correlation profiles in Fig. 10b become generally more consistent with the expectation that a stronger tropical cyclone will have a warm, moist, high vorticity core in the troposphere and an anticyclone near the tropopause (e.g., Gray 1975; Hawkins and Imbembo 1976; Frank 1977). A notable exception is the large drop in correlation between SLP and midlevel moisture. This particular correlation drops because the averaging area for mixing ratio in Fig. 10b encompasses the tropical cyclone core and areas of subsidence outside the core. Stronger cyclones should have higher moisture in their cores, but they also will be surrounded by more intense subsidence. Thus, by 24 h the smaller averaging area used in the 500–850-hPa layer-mean mixing ratio correlation is a more appropriate predictor of final intensity. Indeed, layer-mean moisture and final intensity in Fig. 9a are moderately correlated. This represents a significant change in dynamics from 12 h, when the two variables are uncorrelated owing to downdrafts.

6. Sensitivity experiments

This section first analyzes some possible impacts of cumulus parameterization on the preceding experiment. Ensemble 30KM is created using the same initial conditions as in CTRL, but only the 30-km domain is used. More importantly, this requires the use of cumulus parameterization. Although using cumulus parameterization is not preferable since the merits of individual cumulus schemes are presently limited (e.g., Arakawa 2004), it is often necessary in the operational environment in which models with grid spacing larger than that in CTRL are used.

Also investigated here are the effects of changing the ensemble initial conditions in 30KM to those that produce generally weaker (WEAK) and stronger (STRG) storms. The purpose of these experiments is to investigate the extent to which genesis dynamics change when both more and fewer ensemble members encompass the truth.

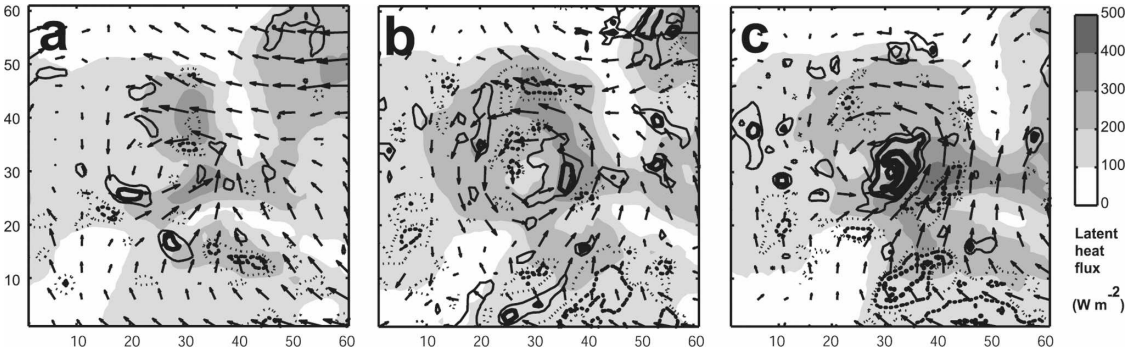

FIG. 15. Ensemble-mean latent heat flux (shaded every 100 W m^{-2}), surface wind vectors (scaled differently in each panel), and instantaneous correlation between latent heat fluxes and intensity for CTRL at (a) 12 h, (b) 24 h, and (c) 36 h. Correlation is contoured at −0.7, −0.5, −0.3, 0.3, 0.5, and 0.7 with solid (dashed) lines indicating positive (negative) correlation and increasing thickness indicating increasing correlation magnitude. All panels are in a Lagrangian framework.

a. Experiment 30KM: Possible effects of cumulus parameterization

As in CTRL, cyclone intensity in 30KM strongly depends upon the strength of cyclogenesis and amount of precipitation during the first 24 h. The correlation between instantaneous SLP and final SLP in Fig. 9d becomes very strong by 24 h, and surface wind speed and vorticity also have strong time-lag relationships by 18 h. Precipitation totals over the first 24 h are also strongly correlated with final SLP, which shows that latent heating during the first 24 h is crucial to cyclogenesis in 30KM.

The vertical correlation profiles in Fig. 10 show that the amount of deep moisture present is also crucial in 30KM. As in CTRL, final storm intensity is weakly to moderately correlated with the initial water vapor mixing ratio throughout nearly the entire troposphere. While the level of maximum correlation is about 100 hPa lower than in CTRL and the magnitude of correlation between mixing ratio and SLP is somewhat lower in 30KM throughout the middle troposphere, these differences are not statistically significant with even 80% confidence.

Convective instability is also important in 30KM, again largely because of its relationship with subsequent precipitation totals. As with CTRL, MUCAPE at the analysis time is moderately correlated with both final SLP and subsequent 24-h precipitation totals. This again provides a direct link between initial MUCAPE and final storm intensity. Also, weak correlation (0.38) between QG lift and MUCAPE suggests that the QG circulation indirectly contributes to cyclogenesis in 30KM as well.

One important difference between CTRL and 30KM is that MUCAPE is positively correlated to final SLP in 30KM for a much longer time. Comparing Fig. 9a with Fig. 9c, the correlation between MUCAPE and SLP in 30KM at 12 h (18 h) is different from that in CTRL with 90% (80%) confidence. The difference is even stronger by 30 h when the two variables are moderately anticorrelated in CTRL and uncorrelated in 30KM. This difference in correlation is significant with more than 99% confidence.

A possible interpretation of this result is that the Grell cumulus parameterization scheme is overly sensitive to CAPE because it relies too heavily on low-level instability to determine where convection should occur. This is supported by the difference in how SLP relates to thermodynamic variables in 30KM and CTRL. In 30KM, 36-h SLP is strongly correlated to the initial temperature within the PBL and moderately to strongly anticorrelated with static stability from within the PBL to between 700 and 800 hPa (Fig. 10c). The correlation in both these relationships is different from its corresponding value in CTRL with 95% confidence. It appears that the strong anticorrelation between static stability and SLP in 30KM is due to the fact that the Grell scheme is generally quite sensitive to the vertical gradient of moist static energy near the top of the PBL (e.g., Cohen 2002).

The difference in how convection is treated in 30KM and CTRL is another possible reason for the discrepancy in correlation between MUCAPE and SLP. Because 30KM tends to produce less widespread stratiform precipitation than CTRL (e.g., Figs. 4 and 6), it is less effective at reducing MUCAPE over a large area. For example, ensemble-mean MUCAPE and surface θ_e (Figs. 13b,c) fall much less in 30KM than in CTRL over the first 12 h. Furthermore, Fig. 7 shows a specific example of how MUCAPE relates to precipitation in CTRL and 30KM at 36 h. The 36-h ensemble-mean precipitation maximum is generally south and east of the mean center in both CTRL and 30KM, but MUCAPE in this area in 30KM is much higher than that in CTRL. Thus, the nature of convection in 30KM appears to less effectively destroy CAPE. Also, as previously mentioned, the correlation between MUCAPE and preceding precipitation in CTRL becomes strongly negative by 30 h, whereas the two variables have no statistically significant relationship at 30 h in 30KM. This difference is significant with more than 99% confidence.

The use of cumulus parameterization might also affect the correlation between initial vorticity and final SLP in 30KM in an unphysical way. Figure 10c shows that initial surface vorticity and final SLP are weakly anticorrelated in 30KM, a counterintuitive result possibly due to the strong anticorrelation between static stability and SLP in 30KM. Area-averaged low-level vorticity is weakly correlated with low-level static stability in 30KM, an expected relationship given the arguments of Hoskins et al. (1985). Therefore, anticorrelation between storm intensity and low-level vorticity might also be expected given the concomitant anticorrelation between storm intensity and low-level static stability. Recall that low-level vorticity is uncorrelated to final intensity in CTRL; the difference in correlation here is significant with about 90% confidence.

Also, the time-lag correlation between instantaneous and final vorticity in 30KM is generally less than it is in CTRL. The difference is most extreme at 6 h (cf. Figs. 9b and 10d), when the correlation is only around 0.1 in 30KM, but it is over 0.8 in CTRL. This is a significant difference with over 99% confidence and indicates that

it takes longer for a coherent vorticity maximum to organize in 30KM than in CTRL.

Deep-layer wind shear remains an important inhibitor to strengthening in 30KM. The evolution of shear is very similar to that in CTRL (Fig. 13d), and as before final intensity is most strongly anticorrelated to shear when shear is highest. Also as in CTRL, the magnitude of shear decreases tremendously between 6 and 18 h. Since 12-h shear in 30KM is strongly anticorrelated with 12-h precipitation totals, the decrease in shear again seems to be the result of deep convection.

Finally, LHF is important in 30KM, but there is some difference from CTRL in its relationship with final SLP. First, the time-lag correlation between LHF and final SLP indicates that LHF again contributes to strengthening before the onset of WISHE (Fig. 9c). As in CTRL, the instantaneous correlation between SLP and LHF increases with time, and it appears that WISHE becomes a factor by about 24–30 h. The major difference between CTRL and 30KM is that the time-lag correlation between SLP and LHF is significantly less in CTRL around 6 h; the reason for this large difference is unclear. Differences between CTRL and 30KM in terms of both time-lag and instantaneous correlation between SLP and LHF continue until about 30 h, but they are not statistically significant.

b. *Experiments WEAK and STRG: The effect of changing initial conditions*

The underlying dynamics in WEAK and STRG have both similarities to and differences with those of 30KM. First, despite the large difference in layer-mean moisture from STRG to WEAK (Fig. 13a), initial deep moisture is significantly correlated with final intensity in both ensembles (Fig. 10). While shear is also an inhibiting factor in both ensembles at different times in Fig. 10, the evolution of correlation between shear and SLP is different than 30KM in both ensembles. The shear to SLP correlation in STRG initially resembles that of 30KM; it becomes significantly positive after 12 h. Meanwhile, shear and final intensity are initially uncorrelated and become more strongly anticorrelated with time in WEAK. These differences in correlation from 30KM are significant with at least 90% confidence by 30 h and, because shear in Fig. 13 is generally similar among the ensembles at later times, they indicate that the effect of shear likely depends on storm intensity. As with shear, the importance of MUCAPE changes with time differently in STRG and WEAK than in 30KM. In WEAK (Fig. 9e), the correlation between MUCAPE and SLP has no net trend, but the correlation between MUCAPE and SLP becomes lower in STRG (Fig. 9g) than in 30KM. The difference in correlation between WEAK (STRG) and 30KM is significant with 90% (80%) confidence by 30 h, and it appears that the time it takes to transition from the CAPE intensification regime also depends on storm intensity. Finally, Fig. 9 shows that the relationship between LHF and final SLP is generally similar in WEAK and STRG to that seen in 30KM. The instantaneous correlation between LHF and SLP rises from insignificant levels at 6 h to moderate and high levels at 30 h. Although the time-lag correlation between LHF and final SLP is weaker in WEAK than STRG with over 95% confidence (cf. Figs. 9e and 9g), the difference quickly decreases with time. Again, the reason for the large difference at early times is unclear.

7. Discussion

The primary intensification mechanism during the first 6–12 h in CTRL is the explosive development of convective towers in a moist, unstable environment of weak QG lift. Figure 12 shows that those ensemble members that have the most initial MUCAPE and deep moisture averaged over a large region around their cyclone centers tend to produce more precipitation both in the immediate vicinity of the centers and over the larger area during the first 6–12 h. The immediate response to the heavy precipitation is a rapid increase in surface wind speeds in the immediate vicinity of the centers, and after 6 h the surface wind speeds in the strongest member are roughly twice those in the weakest member (Fig. 12f).

The intensification rate subsides dramatically for all members by 12 h, likely because prolific downdrafts stabilize the lower troposphere (Figs. 12c–e). Large-area-averaged surface θ_e reaches a minimum around 12 h, but the time of absolute minimum θ_e in the vicinity of the centers varies from 6 h in member 6 to 24 h in member 19. In response to the stabilization, precipitation rates plateau or fall significantly, depending on the ensemble member and averaging area.

Precipitation rates increase again when surface θ_e recovers after 24–30 h near the centers of convectively active members. This is approximately the time that the ensemble statistics support the WISHE mechanism becoming a dominant intensification factor. Concomitant with the increase in precipitation and onset of WISHE, the rate of intensification begins to accelerate, a tendency most strongly seen in member 6. Downdrafts still affect the minimum θ_e when precipitation intensifies from 24 to 36 h (cf. Figs. 10b and 10d), but not to the extent of the earlier downdrafts.

Since MUCAPE and deep moisture are responsible for vortex spinup before 12 h, they ultimately help de-

termine the intensity of the final cyclone. For example, the correlation analysis in Fig. 9 shows that SLP variations at 12 h account for nearly 65% of the variance in intensity at 36 h. Although it is well known that convective instability does not contribute to the strength of very intense tropical cyclones (e.g., Persing and Montgomery 2005), convective instability here infuses energy into the system *before* WISHE begins. After 12 h it appears that pre-WISHE surface heat fluxes and eventually WISHE itself amplify the 12-h differences, resulting in large ensemble spread.

The importance of initial deep moisture here agrees with numerous other tropical cyclone modeling and observational studies, but how the importance of CAPE relates to other findings is unclear. On one hand, Montgomery et al. (2006) found that VHTs "compete" with one another for ambient CAPE. However, the correlations computed in the current study use area averages much larger than the scale of individual VHTs. It is possible that higher CAPE in this particular case generally favors stronger and/or more numerous VHTs, which in turn incrementally contribute to system-scale heating and vortex spinup, but such details are beyond the scope of this study. On the other hand, the idealized results of Nolan et al. (2007) suggest no relationship between environmental CAPE and the rate of cyclone development in an otherwise favorable environment. One important difference between the current study and theirs is the complete lack of vertical wind shear in their idealized case. As previously noted, modest vertical wind shear is present in the ensembles here, so perhaps CAPE becomes more important in instances where vertical wind shear is also present. Regardless, it is clear that larger-scale thermodynamics are important for cyclogenesis here. This result is similar to Bister and Emanuel (1997) and Nolan (2007), though the destabilization and/or moistening mechanisms here are different than in those studies.

Finally, it is important to note that these results do not imply that CAPE or MUCAPE is a good predictor of tropical cyclone formation in general. Aside from the results of Nolan et al. (2007), it is well known that convective instability in the tropics is often anticorrelated with convective coverage simply because convection tends to stabilize the atmosphere. Because tropical disturbances need sustained, widespread convection to intensify into tropical cyclones, there should not be correlation between CAPE and cyclogenesis occurrences. Also, these results do not imply that additional CAPE can somehow compensate for an unfavorable environment, such as a lack of low-level vorticity, dry midlevels, or excessive shear. Rather, they imply that when other parameters are favorable to neutral (as was the case here), it is *possible* for additional CAPE to speed up the cyclogenesis process.

8. Conclusions

Through methodology unique for tropical cyclones in peer-reviewed literature, this study uses ensemble forecasts to explore the predictability and dynamics of tropical cyclogenesis in the MM5 model. The methods used herein are largely congruent with those of HZ07, but this study takes a step further by investigating the sensitivity of predictability and dynamics to cumulus parameterization and small changes to the initial ensemble mean that produce ensembles of weak and strong cyclones. Large discrepancies among MM5 ensemble members by 36 h reveal considerable forecast uncertainty despite only subtle differences in initial conditions among the members.

This study has pinpointed the source of spread in an ensemble forecast of a tropical cyclone; to the knowledge of the authors, this has never before been accomplished. It has been demonstrated that the two most important factors in the initial conditions for genesis in this case are the presence of deep moisture and high CAPE. These factors combine to yield more active initial convection and a quick spinup during the first 6–12 h. Because these factors result in quicker genesis in some ensemble members than others, they are also the primary source for spread early in the ensemble. Discrepancies after 12 h are amplified by differences in convection that are related to fluxes of sensible and latent heat. Eventually the WISHE mechanism results in even larger ensemble spread. Although CAPE certainly is not a dominant factor here, it appears that it may be relevant in some circumstances, perhaps in sheared environments.

Although using cumulus parameterization and changing the initial ensemble mean produces qualitatively similar results, such changes can significantly modulate how quickly an ensemble moves out of the CAPE-based intensification regime and when shear becomes an important factor. The Grell scheme is strongly sensitive to lower-tropospheric temperature and static stability, and it affects the nature of convection, resulting in less stratiform precipitation and more deep convective cells. This convection with Grell does not remove MUCAPE as effectively as high-resolution, explicit convection, and MUCAPE therefore contributes to intensification in 30KM for a longer period of time than it does in CTRL. Meanwhile, in STRG (WEAK) MUCAPE stays correlated with final intensity for less (more) time than in 30KM. Finally, shear negatively affects storm intensity in WEAK at a much later time than in the other ensembles.

Also, it appears that cumulus parameterization can appreciably change the ensemble spread. In this situation, there is a fair amount more spread in 30KM than in CTRL in terms of RM-DTE over the entire domain. The discrepancy is accentuated in the region of the ensemble mean position of the cyclone at 36 h, where the peak in RM-DTE in 30KM is nearly double that in CTRL. This difference in spread is likely intimately related to differences in the nature of convection between CTRL and 30KM.

Finally, this study is meant only as a starting point to investigate the dynamics of the 2004 case. These results can be used to investigate both the evolution of certain variables within individual members of the ensembles and to perform more advanced statistical analysis. Also, this study has the limitation of investigating only one case. Preliminary investigations into other tropical cyclogenesis cases not presented here show that the development of different disturbances can depend on a variety of similar and dissimilar factors.

Acknowledgments. This research was completed as part of J. A. Sippel's doctoral dissertation at Texas A&M University. This research is sponsored by NSF Grant ATM0205599 and by the Office of Navy Research under Grant N000140410471. The authors are grateful to David Nolan, who reviewed the paper, and two other anonymous reviewers. John Nielsen-Gammon, Chris Snyder, Mike Montgomery, Tim Dunkerton, Courtney Schumacher, Scott Braun, Kevin Tory, and Dan Hawblitzel also provided comments beneficial to this study.

REFERENCES

Aberson, S. D., 2001: The ensemble of tropical cyclone track forecasting models in the North Atlantic basin (1976–2000). *Bull. Amer. Meteor. Soc.,* **82,** 1895–1904.

Arakawa, A., 2004: The cumulus parameterization problem: Past, present, and future. *J. Climate,* **17,** 2493–2525.

Barker, D. M., W. Huang, Y.-R. Guo, A. J. Bourgeois, and Q. N. Xiao, 2004: A three-dimensional variational data assimilation system for MM5: Implementation and initial results. *Mon. Wea. Rev.,* **132,** 897–914.

Bender, M. A., I. Ginis, and Y. Kurihara, 1993: Numerical simulations of tropical cylone–ocean interaction with a high-resolution coupled model. *J. Geophys. Res.,* **98,** 23 245–23 263.

Bister, M., and K. A. Emanuel, 1997: The genesis of Hurricane Guillermo: TEXMEX analyses and a modeling study. *Mon. Wea. Rev.,* **125,** 2662–2682.

Black, P. G., 1983: Ocean temperature changes induced by tropical cyclones. Ph.D. dissertation, The Pennsylvania State University, 278 pp.

Braun, S., 2006: High-resolution simulation of Hurricane Bonnie (1998). Part II: Water budget. *J. Atmos. Sci.,* **63,** 43–64.

——, M. T. Montgomery, and Z. Pu, 2006: High-resolution simulation of Hurricane Bonnie (1998). Part I: The organization of eyewall vertical motion. *J. Atmos. Sci.,* **63,** 19–42.

Cohen, C., 2002: A comparison of cumulus parameterizations in idealized sea-breeze simulations. *Mon. Wea. Rev.,* **130,** 2554–2571.

Davis, C. A., and L. F. Bosart, 2002: Numerical simulations of the genesis of Hurricane Diana (1984). Part II: Sensitivity of track and intensity prediction. *Mon. Wea. Rev.,* **130,** 1100–1124.

DeMaria, M., and J. M. Gross, 2003: Evolution of prediction models. *Hurricane! Coping with Disaster: Progress and Challenges since Galveston, 1900,* R. Simpson, Ed., Amer. Geophy. Union, 103–126.

——, J. A. Knaff, and B. H. Connell, 2001: A tropical cyclone genesis parameter for the tropical Atlantic. *Wea. Forecasting,* **16,** 219–233.

——, M. Mainelli, L. K. Shay, J. A. Knaff, and J. Kaplan, 2005: Further improvements to the Statistical Hurricane Intensity Prediction Scheme (SHIPS). *Wea. Forecasting,* **20,** 531–543.

Doswell, C. A., III, and E. N. Rasmussen, 1994: The effect of neglecting the virtual temperature correction on CAPE calculations. *Wea. Forecasting,* **9,** 625–629.

Dudhia, J., 1993: A nonhydrostatic version of the Penn State–NCAR Mesoscale Model: Validation tests and simulation of an Atlantic cyclone and cold front. *Mon. Wea. Rev.,* **121,** 1493–1513.

Dunion, J. P., and C. S. Velden, 2004: The impact of the Saharan air layer on Atlantic tropical cyclone activity. *Bull. Amer. Meteor. Soc.,* **85,** 353–365.

Elsberry, R. L., T. D. B. Lambert, and M. A. Boothe, 2007: Accuracy of Atlantic and eastern North Pacific tropical cyclone intensity forecast guidance. *Wea. Forecasting,* **22,** 747–762.

Emanuel, K. A., 1986: An air–sea interaction theory for tropical cyclones. Part I: Steady-state maintenance. *J. Atmos. Sci.,* **43,** 585–604.

——, 1989: The finite-amplitude nature of tropical cyclogenesis. *J. Atmos. Sci.,* **46,** 3431–3456.

——, 1995: Sensitivity of tropical cyclones to surface exchange coefficients and a revised steady-state model incorporating eye dynamics. *J. Atmos. Sci.,* **52,** 3969–3976.

——, 2003: A century of scientific progress: An evaluation. *Hurricane! Coping with Disaster: Progress and Challenges since Galveston, 1900,* R. Simpson, Ed., American Geophysical Union, 177–204.

——, J. D. Neelin, and C. S. Bretherton, 1994: On large-scale circulations in convecting atmospheres. *Quart. J. Roy. Meteor. Soc.,* **120,** 1111–1144.

Frank, W. M., 1977: The structure and energetics of the tropical cyclone. I. Storm structure. *Mon. Wea. Rev.,* **105,** 1119–1135.

Franklin, J. L., 2005: 2004 National Hurricane Center forecast verification report. 46 pp. [Available online at http://www.nhc.noaa.gov/verification/pdfs/Verification_2004.pdf.]

Goerss, J. S., 2000: Tropical cyclone track forecasts using an ensemble of dynamical models. *Mon. Wea. Rev.,* **128,** 1187–1193.

Gray, W. M., 1968: Global view of the origin of tropical disturbances and storms. *Mon. Wea. Rev.,* **96,** 669–700.

——, 1975: Tropical cyclone genesis. Colorado State University Department of Atmospheric Sciences Paper 323, 121 pp. [Available from the Department of Atmospheric Sciences, Colorado State University, Ft. Collins, CO 80523.]

Grell, G. A., 1993: Prognostic evaluation of assumptions used by cumulus parameterizations. *Mon. Wea. Rev.,* **121,** 764–787.

——, Y.-H. Kuo, and R. Pasch, 1991: Semiprognostic tests of cumulus parameterization schemes in the middle latitudes. *Mon. Wea. Rev.,* **119,** 5–31.

Hakim, G. J., and R. D. Torn, 2008: Ensemble synoptic analysis. *Synoptic–Dynamic Meteorology and Weather Analysis and Forecasting: A Tribute to Fred Sanders, Meteor. Monogr.,* Amer. Meteor. Soc., in press.

Harr, P. A., R. L. Elsberry, and J. C. Chan, 1996: Transformation of a large monsoon depression to a tropical storm during TCM-93. *Mon. Wea. Rev.,* **124,** 2625–2643.

Hawblitzel, D. P., F. Zhang, Z. Meng, and C. A. Davis, 2007: Probabilistic evaluation of the dynamics and predictability of the mesoscale convective vortex of 10–13 June 2003. *Mon. Wea. Rev.,* **135,** 1544–1563.

Hawkins, H. F., and S. M. Imbembo, 1976: The structure of a small, intense hurricane—Inez 1966. *Mon. Wea. Rev.,* **104,** 418–442.

Hendricks, E. A., M. T. Montgomery, and C. A. Davis, 2004: The role of "vortical" hot towers in the formation of tropical cyclone Diana (1984). *J. Atmos. Sci.,* **61,** 1209–1232.

Hoskins, B. J., M. E. McIntyre, and A. W. Robertson, 1985: On the use and significance of isentropic potential vorticity maps. *Quart. J. Roy. Meteor. Soc.,* **111,** 877–946.

Houze, R. A., S. S. Chen, B. F. Smull, W.-C. Lee, and M. M. Bell, 2007: Hurricane intensity and eyewall replacement. *Science,* **315,** 1235–1239.

Islam, S., R. L. Bras, and K. A. Emanuel, 1993: Predictability of mesoscale rainfall in the tropics. *J. Appl. Meteor.,* **32,** 297–310.

Krishnamurti, T. N., R. Correa-Torres, G. Rohaly, D. Oosterhof, and N. Surgi, 1997: Physical initialization and hurricane ensemble forecasts. *Wea. Forecasting,* **12,** 503–514.

——, C. M. Kishtawal, Z. Zhang, T. LaRow, D. Bachiochi, E. Williford, S. Gadgil, and S. Surendran, 2000: Multimodel ensemble forecasts for weather and seasonal climate. *J. Climate,* **13,** 4196–4216.

——, S. Pattnaik, L. Stefanova, T. S. V. Vijaya Kumar, B. P. Mackey, A. J. O'Shay, and R. J. Pasch, 2005: The hurricane intensity issue. *Mon. Wea. Rev.,* **133,** 1886–1912.

Mackey, B. P., and T. N. Krishnamurti, 2001: Ensemble forecast of a typhoon flood event. *Wea. Forecasting,* **16,** 399–415.

Mapes, B. E., T. T. Warner, M. Xu, and D. J. Gochis, 2004: Comparison of cumulus parameterizations and entrainment using domain-mean wind divergence in a regional model. *J. Atmos. Sci.,* **61,** 1284–1295.

McBride, J. L., and R. Zehr, 1981: Observational analysis of tropical cyclone formation. Part II: Comparison of non-developing versus developing systems. *J. Atmos. Sci.,* **38,** 1132–1151.

Mellor, G. L., and T. Yamada, 1982: Development of a turbulence closure model for geophysical fluid problems. *Rev. Geophys.,* **20,** 851–875.

Meng, Z., and F. Zhang, 2007: Tests of an ensemble Kalman filter for mesoscale and regional-scale data assimilation. Part II: Imperfect model experiments. *Mon. Wea. Rev.,* **135,** 1403–1423.

Mitchell, H. L., P. L. Houtekamer, and G. Pellerin, 2002: Ensemble size, balance, and model-error representation in an Ensemble Kalman Filter. *Mon. Wea. Rev.,* **130,** 2791–2808.

Montgomery, M. T., M. E. Nicholls, T. A. Cram, and A. B. Saunders, 2006: A vortical hot tower route to tropical cyclogenesis. *J. Atmos. Sci.,* **63,** 355–386.

NOAA SSD, cited 2008: Tropical cyclone formation probability guidance product. NOAA Satellite Services Division. [Available online at http://www.ssd.noaa.gov/PS/TROP/TCFP/index.html.]

Nolan, D. S., 2007: What is the trigger for tropical cyclogenesis? *Aust. Meteor. Mag.,* **56,** 241–266.

——, E. D. Rappin, and K. A. Emanuel, 2007: Tropical cyclogenesis sensitivity to environmental parameters in radiative–convective equilibrium. *Quart. J. Roy. Meteor. Soc.,* **133,** 2085–2107.

Olson, D. A., N. W. Junker, and B. Korty, 1995: Evaluation of 33 years of quantitative precipitation forecasting at the NMC. *Wea. Forecasting,* **10,** 498–511.

Park, K., and X. Zou, 2004: Toward developing an objective 4DVAR BDA scheme for hurricane initialization based on TPC observed parameters. *Mon. Wea. Rev.,* **132,** 2054–2069.

Persing, J., and M. T. Montgomery, 2005: Is environmental CAPE important in the determination of maximum possible hurricane intensity? *J. Atmos. Sci.,* **62,** 542–550.

Raymond, D. J., C. Lopez-Carrillo, and L. L. Cavazos, 1998: Case studies of developing East Pacific easterly waves. *Quart. J. Roy. Meteor. Soc.,* **124,** 2005–2034.

Reasor, P. D., M. T. Montgomery, and L. F. Bosart, 2005: Mesoscale observations of the genesis of Hurricane Dolly (1996). *J. Atmos. Sci.,* **62,** 3151–3171.

Reisner, J., R. M. Rasmussen, and R. T. Bruintjes, 1998: Explicit forecasting of supercooled liquid water in winter storms using the MM5 mesoscale model. *Quart. J. Roy. Meteor. Soc.,* **124B,** 1071–1107.

Riehl, H., 1954: *Tropical Meteorology.* McGraw-Hill, 392 pp.

Ritchie, E. A., and G. J. Holland, 1997: Scale interactions during the formation of Typhoon Irving. *Mon. Wea. Rev.,* **125,** 1377–1396.

Rotunno, R., and K. A. Emanuel, 1987: An air–sea interaction theory for tropical cyclones. Part II: Evolutionary study using a nonhydrostatic axisymmetric numerical model. *J. Atmos. Sci.,* **44,** 542–561.

Simpson, J., E. Ritchie, G. J. Holland, J. Halverson, and S. Stewart, 1997: Mesoscale interactions in tropical cyclone genesis. *Mon. Wea. Rev.,* **125,** 2643–2661.

Sippel, J. A., J. W. Nielsen-Gammon, and S. E. Allen, 2006: The multiple-vortex nature of tropical cyclogenesis. *Mon. Wea. Rev.,* **134,** 1796–1814.

Snyder, C., and F. Zhang, 2003: Assimilation of simulated Doppler radar observations with an ensemble Kalman filter. *Mon. Wea. Rev.,* **131,** 1663–1677.

Tory, K. J., M. T. Montgomery, and N. E. Davidson, 2006a: Prediction and diagnosis of tropical cyclone formation in an NWP system. Part I: The critical role of vortex enhancement in deep convection. *J. Atmos. Sci.,* **63,** 3077–3089.

——, ——, N. D. Davidson, and J. D. Kepert, 2006b: Prediction and diagnosis of tropical cyclone formation in an NWP system. Part II: A diagnosis of Tropical Cyclone Chris formation. *J. Atmos. Sci.,* **63,** 3091–3113.

Vijaya Kumar, T. S. V., T. N. Krishnamurti, M. Fiorino, and M. Nagata, 2003: Multimodel superensemble forecasting of tropical cyclones in the Pacific. *Mon. Wea. Rev.,* **131,** 574–583.

Weber, H. C., 2003: Hurricane track prediction using a statistical ensemble of numerical models. *Mon. Wea. Rev.,* **131,** 749–770.

——, 2005a: Probabilistic prediction of tropical cyclones. Part I: Position. *Mon. Wea. Rev.,* **133,** 1840–1852.

——, 2005b: Probabilistic prediction of tropical cyclones. Part II: Intensity. *Mon. Wea. Rev.,* **133,** 1853–1864.

Williford, C. E., T. N. Krishnamurti, R. C. Torres, S. Cocke, Z.

Christidis, and T. S. V. Vijaya Kumar, 2003: Real-time multimodel superensemble forecasts of Atlantic tropical systems of 1999. *Mon. Wea. Rev.,* **131,** 1878–1894.

Wu, C.-C., K.-H. Chou, Y. Wang, and Y.-H. Kuo, 2006: Tropical cyclone initialization and prediction based on four-dimensional variational data assimilation. *J. Atmos. Sci.,* **63,** 2383–2395.

Zhang, F., 2005: Dynamics and structure of mesoscale error covariance of a winter cyclone estimated through short-range ensemble forecasts. *Mon. Wea. Rev.,* **133,** 2876–2893.

——, C. Snyder, and R. Rotunno, 2002: Mesoscale predictability of the "surprise" snowstorm of 24–25 January 2000. *Mon. Wea. Rev.,* **130,** 1617–1632.

——, ——, and ——, 2003: Effects of moist convection on mesoscale predictability. *J. Atmos. Sci.,* **60,** 1173–1185.

——, A. M. Odins, and J. W. Nielsen-Gammon, 2006a: Mesoscale predictability of an extreme warm-season precipitation event. *Wea. Forecasting,* **21,** 149–166.

——, Z. Meng, and A. Aksoy, 2006b: Tests of an ensemble Kalman filter for mesoscale and regional-scale data assimilation. Part 1: Perfect model experiments. *Mon. Wea. Rev.,* **134,** 722–736.

——, N. Bei, R. Rotunno, C. Snyder, and C. C. Epifanio, 2007: Mesoscale predictability of moist baroclinic waves: Convection-permitting experiments and multistage error growth dynamics. *J. Atmos. Sci.,* **64,** 3579–3594.

Zhang, Z., and T. N. Krishnamurti, 1999: A perturbation method for hurricane ensemble predictions. *Mon. Wea. Rev.,* **127,** 447–469.